Available online at www.sciencedirect.com
SCIENCE DIRECT®
PERGAMON
Polyhedron 22 (2003) 1585–1593
POLYHEDRON
www.elsevier.com/locate/poly

The synthesis and characterization of three oxidized derivatives of bis(diphenylphosphino)pyridine and their Sn(IV) complexes

Richard Sevcik, Marek Necas, Josef Novosad *

Faculty of Science, Department of Inorganic Chemistry, Masaryk University, Kotlarska 2, CZ-61137 Brno, Czech Republic

Received 6 January 2003; accepted 24 March 2003

Dedicated to Professor Steinar Husebye, Department of Chemistry, University of Bergen (Norway), on the occasion of his 70th birthday

Abstract

The synthesis and spectroscopic characterization of three chalcogenophosphoryl ligands derived from pyridine is reported. The synthesis was based on the oxidation of $C_5H_3N(PPh_2)_2$ by elemental sulfur and selenium, and hydrogen peroxide. As a part of our study on the coordination chemistry of the ligands, three new Sn(IV) complex cations of the general formula $\{[Ph_2P(E)\text{-}C_5H_3N\text{-}P(E)Ph_2]SnCl_3\}^+$ (E = O, S, Se) were also synthesized. All compounds were characterized by ^{31}P NMR and X-ray crystallography. The organic ligands are tridentate, with both chalcogens and nitrogen involved in chelation. The cations show an approximate octahedral core geometry and are paired with either $SnCl_5^-$ or $SnCl_5(OH_2)^-$ anions.

Keywords: Diphosphino ligands; Chalcogens; Pyridine; Tin(IV); X-ray crystallography

1. Introduction

Research in the area of organophosphorus derivatives of pyridine has focused mainly on bis(diphenylphosphino)pyridine (bppp) [1]. Bis(diphenylphosphino)pyridine is relatively easily oxidized on both its terminal phosphorus atoms and bis(diphenylphosphoryl)pyridine was first described in 1978 [2], and the thio and seleno analogues are known since 1990 [3]. Nevertheless, a search of the Cambridge structural database [4] reveals only few examples of coordination compounds of bppp but no examples of complexes derived from $[Ph_2P(E)\text{-}C_5H_3N\text{-}P(E)Ph_2]$ (E = O, S, Se) or the ligand itself. Surprisingly, there is no occurrence of bppp. Oxidized bppp derivatives can be considered as the pyridine analogues of tetraphenylimidodiphosphinates $Ph_2P(E)\text{-}NH\text{-}P(E)Ph_2$ (E = O, S, Se) which were found to be excellent ligands after deprotonation through the coordination via the lone pairs of the chalcogen to the metal [5]. Comparing to imidodiphosphinates the bppp derivatives might be expected to be less flexible due to their central rigid part and the neighboring sterically demanding phenyl groups. Here we report the preparation of oxidized derivatives of bppp and their Sn(IV) complexes and investigations into the crystal and molecular structures.

2. Experimental

All reactions were performed under argon in anhydrous conditions using conventional Schlenk techniques with the exception of hydrogen peroxide oxidation. All chemicals were used as supplied and solvents were dried by standard methods and were distilled prior to use [6]. ^{31}P NMR spectra were recorded in CH_2Cl_2 using a Bruker AVANCE DRX 300 instrument and were referenced to H_3PO_4 (85%). IR spectra were recorded on Nujol mulls using a Bruker IFS 28 spectrometer. Microanalyses were performed using a Fisons EA 1108 instrument at the Palacky University, Olomouc, Czech Republic.

* Corresponding author. Tel.: +420-5-41129325; fax: +420-5-41211214.
E-mail address: novosad@chemi.muni.cz (J. Novosad).

0277-5387/03/$ - see front matter
doi:10.1016/S0277-5387(03)00291-2

3. Ligands synthesis

3.1. $(Ph_2P)_2C_5NH_3$ (bppp, **1**)

A solution of triphenylphosphine (46.3 g, 0.177 mol) in anhydrous tetrahydrofuran (thf) (75 ml) was added over 1.5 h into a solution of sodium metal (8.2 g, 0.357 mol) in liquid ammonia (400 ml) while stirring and the reaction was continued for 1 h. Then, ammonium chloride (9.5 g, 0.177 mol) was added in small portions. After 1.5 h, a solution of 2,6-difluoropyridine (7.8 ml, 86 mmol) was added dropwise over 1 h and stirring was maintained for the next 1 h. Finally, toluene (150 ml) was added and the reaction mixture was left standing overnight at room temperature to evaporate excess ammonia. The mixture was then refluxed until no ammonia vapors were detected. After all solvents were removed by distillation and replaced by dichloromethane (350 ml), the insoluble solid was filtered-off. Then, the volume of dichloromethane was reduced by half and methanol was added (120 ml). The procedure was completed by gradual elimination of the remaining dichloromethane leading to precipitation of bppp, which was collected by filtration and dried in vacuo. Yield: 25.1 g (65%). Anal. Found: C, 78.3; H, 5.2; N, 3.5. Calc. for $C_{29}H_{23}NP_2$: C, 77.8; H, 5.2; N, 3.2%. m.p.: 124–125 °C. IR: 3071 w, 3056 w, 3025 w, 1546 s, 1478 m, 1434 s, 1421 s, 1094 m, 748 vs, 694 vs, 504 m, 496 m, 485 m, 465 m. $^{31}P\{^1H\}$ NMR: δ −2.8 singlet (see Fig. 1).

3.2. $[Ph_2P(O)]_2C_5NH_3$ ($bpppO_2$, **2**)

A solution of **1** (5.0 g, 11 mmol) in anhydrous thf (50 ml) was cooled to 10 °C and hydrogen peroxide (30%, 6 ml, 58 mmol) was added dropwise over 30 min and then the reaction mixture was left stirring at room temperature for 1.5 h. A white suspension was concentrated in vacuo and diethylether (100 ml) was added to give a white solid. Yield: 5.2 g (97%). Anal. Found: C, 69.4; H, 4.9; N, 3.1. Calc. for $C_{29}H_{23}NP_2O_2\cdot H_2O_2$: C, 67.8; H, 4.9; N, 2.7%. m.p.: 229–230 °C. IR: 3518 m, 3429 m, 3294 w, 3198 w, 3074 w, 3057 w, 1666 m, 1437 s, 1188 s, 1164 m, 1123 m, 876 vw, 722 m, 706 m, 695 m, 556 s, 539 m, 526 vs, 502 w. $^{31}P\{^1H\}$ NMR: δ 21.3 singlet (see Fig. 2).

3.3. $[Ph_2P(S)]_2C_5NH_3$ ($bpppS_2$, **3**)

1 (5.0 g, 11 mmol) was dissolved in toluene (125 ml) and sulfur (0.72 g, 22 mmol) was added. After 8 h of refluxing, the mixture was cooled to room temperature and a white solid was filtered-off and washed with methanol. The filtrate was concentrated in vacuo to approximately 35 ml and stored at −20 °C overnight; another fraction of product was collected by filtration, washed with methanol and dried. Yield (sum): 4.98 g (89%). Anal. Found: C, 66.5; H, 3.5; N, 2.6; S, 11.0. Calc. for $C_{29}H_{23}NP_2S_2$: C, 68.0; H, 4.5; N, 2.7; S, 12.5%. m.p.: 204–205 °C. IR: 3076 vw, 3059 w, 3049 vw, 1560 m, 1437 vs, 1108 s, 1102 s, 987 m, 808 s, 799 m, 743 s, 720 vs, 694 vs, 647 vs, 521 vs, 510 s, 492 s, 481 m, 469 w, 451 w, 412 vw. $^{31}P\{^1H\}$ NMR: δ 38.9 singlet (see Fig. 3).

3.4. $[Ph_2P(Se)]_2C_5NH_3$ ($bpppSe_2$, **4**)

1 (4.87 g, 11 mmol) was dissolved in toluene (140 ml) and grey selenium powder (1.75 g, 22 mmol) was added. After 18 h of refluxing, excess selenium was removed by filtration, the mixture was cooled to room temperature and colorless crystals were filtered-off, washed with methanol and dried. The filtrate, concentrated to approximately 35 ml, was stored at −20 °C overnight to yield the second fraction of product. The white solid was filtered-off, washed with methanol and dried. Yield (sum): 5.41 g (81%). Anal. Found: C, 58.1; H, 3.8; N, 2.3. Calc. for $C_{29}H_{23}NP_2Se_2$: C, 57.6; H, 3.8; N, 2.3%. m.p.: 241–242 °C. IR: 3073 vw, 3053 w, 3048 vw, 1556 m, 1480 m, 1436 vs, 1425 m, 1372 m, 1309 w, 1157 w, 1100 s, 986 m, 804 m, 795 m, 742 s, 703 s, 692 vs, 618 w, 574 vs, 563 s, 515 s, 505 s, 482 s, 445 m, 410 w. $^{31}P\{^1H\}$ NMR: δ 33.1 singlet, ^1J[P–Se] 748.5 Hz (see Fig. 4).

4. Complexes synthesis

4.1. $[SnCl_3\{[Ph_2P(O)]_2C_5NH_3\}][SnCl_5(H_2O)]$ (**5**)

A solution of tin tetrachloride (0.2 ml, 1.56 mmol) in CH_2Cl_2 (5 ml) was dropped into a solution of **2** (0.40 g, 0.78 mmol) in CH_2Cl_2 (10 ml) over 10 min. The reaction mixture was left stirring over 12 h and a white solid was filtered-off. The filtrate was concentrated to approximately 7 ml. A white solid was then collected by filtration, washed with diethylether and dried. Yield: 0.74 g (85%). Anal. Found: C, 32.8; H, 2.5; N, 1.3. Calc. for $C_{29}H_{25}Cl_8NO_3P_2Sn_2\cdot CH_2Cl_2$: C, 32.7; H, 2.5; N, 1.3%. m.p.: 193–198 °C (decomposition). IR: 3057 w, 1589 m, 1460 m, 1437 s, 1375 m, 1268 w, 1166 w, 1120 vs, 1048 s, 1021 s, 995 m, 812 m, 742 s, 729 m, 700 m, 686 s, 614 w, 577 m, 556 vs, 517 vs, 431 w. $^{31}P\{^1H\}$ NMR: δ 36.2 singlet, ^2J[P–Sn] 112.8 Hz.

4.2. $[SnCl_3\{[Ph_2P(S)]_2C_5NH_3\}][SnCl_5]$ (**6**)

A solution of tin tetrachloride (0.17 ml, 1.47 mmol) in CH_2Cl_2 (8 ml) was added over 10 min into a solution of **3** (0.38 g, 0.73 mmol) in CH_2Cl_2 (12 ml). After being stirred for 12 h, the solution was concentrated in vacuo to approximately 4 ml and diethylether (12 ml) was added. A white solid was collected by filtration, washed with diethylether and dried. Yield: 0.75 g (91%). Anal. Found: C, 32.3; H, 2.3; N, 1.2. Calc. for $C_{29}H_{23}Cl_8NP_2S_2Sn_2\cdot CH_2Cl_2$: C, 32.2; H, 2.2; N, 1.3%.

m.p.: 143–147 °C (decomposition). IR: 3056 w, 1610 w, 1583 w, 1562 w, 1458 m, 1440 s, 1377 m, 1335 w, 1312 w, 1256 w, 1194 w, 1104 s, 1096 s, 1010 m, 996 m, 792 m, 746 m, 738 m, 721 m, 710 m, 685 s, 622 s, 606 s, 580 w, 514 vs, 491 s. $^{31}P\{^{1}H\}$ NMR: δ 47.0 singlet, ^{2}J[P–Sn] 86.9 Hz.

4.3. $[SnCl_3\{[Ph_2P(Se)]_2C_5NH_3\}][SnCl_5]$ (7)

A solution of tin tetrachloride (0.15 ml, 1.24 mmol) in CH_2Cl_2 (10 ml) was added over 10 min into a solution of **4** (0.38 g, 0.62 mmol) in CH_2Cl_2 (15 ml); the reaction mixture turned to yellow. After being stirred for 12 h, the solution was concentrated in vacuo to approximately 7 ml and diethylether (10 ml) was added. A pale yellow solid was filtered-off, washed with diethylether and dried. Yield: 0.67 g (90%). Anal. Found: C, 29.9; H, 2.1; N, 1.2. Calc. for $C_{29}H_{23}Cl_8NP_2Se_2Sn_2 \cdot 1.5CH_2Cl_2$: C, 29.2; H, 2.1; N, 1.1%. m.p.: 140–145 °C (decomposition). IR: 3050 w, 1585 w, 1558 w, 1437 vs, 1335 w, 1312 w, 1192 w, 1098 s, 1071 w, 996 m, 794 w, 743 s, 703 s, 687 s, 617 w, 573 m, 552 s, 516 m, 504 s, 483 m, 445 w. $^{31}P\{^{1}H\}$ NMR: δ 44.3 singlet, ^{1}J[P–Se] 580.8 Hz, ^{2}J[P–Sn] 114.7 Hz, ^{1}J[P–C] 81.4 Hz.

5. Crystallography

Diffraction data were collected on a KUMA KM-4 κ-axis diffractometer with graphite-monochromated Mo Kα radiation ($\lambda = 0.71073$ Å) equipped with a CCD detector. The intensity data were corrected for Lorentz and polarization effects. All the structures were solved by direct methods and refined by full-matrix least-squares methods using anisotropic thermal parameters for the non-hydrogen atoms. The software packages used were Xcalibur CCD system [7] for the data collection/reduction, and ShelXTL [8] for the structure solution, refinement and drawing preparation (thermal ellipsoids are drawn at the 50% probability level). Details of the data collection, cell determination and structure refinement are listed in Table 1.

6. Results and discussion

The synthesis of bppp was based on the reported method [3]; however, a new way of product isolation was designed leading to an increased reaction yield of 65% (lit. approximately 40%). After the reaction was complete, the solvent was replaced by dichloromethane and the insoluble sodium fluoride was filtered-off. The product was then precipitated from dichloromethane solution in the pure form by addition of methanol. In the method reported previously, after evaporation of toluene, the oily residue was repeatedly triturated with methanol to obtain the crude product. The oxidized derivatives of bppp were prepared by direct oxidation using either hydrogen peroxide or elementary sulfur or selenium (Eq. (1)). We suggested toluene as a solvent for synthesis of dithio and diseleno derivatives to shorten reaction times; moreover, this alteration led to a simplified isolation of pure products in high yields. In contrast to the method described previously, the products are now obtained as crystalline solids directly from the reaction mixtures. ^{31}P NMR spectra of ligands show singlets with splitting due to ^{31}P–^{77}Se coupling in the case of **4**. Characteristic bands observed in the FTIR for P=E bonds correspond to literature values [2,3].

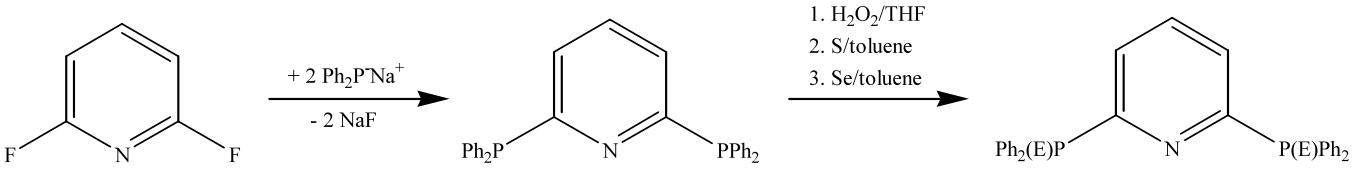

E = O (**2**), S (**3**), Se (**4**) (1)

All manipulations during the tin complexes syntheses (Eq. (2)) were made in strictly anhydrous conditions due to extreme hygroscopicity of tin tetrachloride. All complexes prepared are unstable in solution when exposed to moisture/oxygen or higher temperatures and decompose back to the starting ligands as indicated by the ^{31}P NMR spectra. As expected, the stability of the tin complexes decreases from **5** to **7** in accordance with increasing "softness" of the donor chalcogen atoms in the ligands. Melting points of Sn(IV) complexes are not sharp and the compounds decompose when melting.

Table 1
Crystal data and refinement parameters

	1	2	3	4	5	6	7
Empirical formula	$C_{29}H_{23}NP_2$	$C_{29}H_{25}NO_4P_2$	$C_{29}H_{23}NP_2S_2$	$C_{29}H_{23}NP_2S_2$	$C_{30}H_{23}Cl_{10}NO_3P_2Sn_2$	$C_{30}H_{25}Cl_{10}NP_2S_2Sn_2$	$C_{30.5}H_{23}Cl_{11}NP_2Se_2Sn_2$
Formula weight	447.42	513.44	511.54	605.34	1099.31	1117.45	1250.69
Temperature (K)	120(2)	120(2)	120(2)	120(2)	120(2)	120(2)	120(2)
Crystal system	monoclinic	triclinic	monoclinic	monoclinic	monoclinic	monoclinic	orthorhombic
Space group	$C2/c$	$P\bar{1}$	$P2_1/c$	$P2_1/c$	$C2/c$	$P2_1/n$	$Pbca$
a (Å)	15.062(3)	10.523(2)	13.209(3)	13.279(3)	35.167(7)	10.767(2)	13.085(3)
b (Å)	13.231(3)	10.925(2)	16.344(3)	16.582(3)	10.515(2)	31.586(6)	18.929(4)
c (Å)	13.026(5)	13.107(3)	12.356(2)	12.355(2)	21.819(4)	12.569(3)	34.366(7)
α (°)		99.88(3)					
β (°)	116.91(3)	104.67(3)	112.31(3)	112.11(3)	98.18(3)	112.89(3)	
γ (°)		116.24(3)					
Volume (Å^3)	2314.8(8)	1235.7(4)	2467.8(8)	2520.4(8)	7986(3)	3966.1(14)	8512(3)
Z	4	2	4	4	8	4	8
Calculated density (Mg m^{-3})	1.284	1.380	1.382	1.595	1.829	1.871	1.952
μ (mm^{-1})	0.205	0.213	0.365	3.080	2.033	2.145	3.675
Crystal size (mm)	0.40 × 0.40 × 0.20	0.60 × 0.40 × 0.40	0.60 × 0.25 × 0.25	0.40 × 0.30 × 0.20	0.50 × 0.50 × 0.40	0.50 × 0.40 × 0.40	0.40 × 0.40 × 0.30
θ range (°)	3.49–24.99	3.33–25.00	3.31–25.00	3.56–25.00	3.37–25.00	3.24–24.46	3.20–25.00
Number of reflections	6978	7767	13780	10137	23864	14283	41888
Independent data	2025	4213	4334	4156	7014	6005	7487
Final R indices [$I > 2\sigma(I)$]	0.0314, 0.0785	0.0329, 0.0833	0.0296, 0.0759	0.0299, 0.0863	0.0498, 0.1099	0.0329, 0.0805	0.0807, 0.1832
$\Delta\rho_{max}/\Delta\rho_{min}$ (e Å^{-3})	0.230 and −0.289	0.358 and −0.339	0.344 and −0.351	0.489 and −0.394	2.064 and −1.426	1.262 and −1.008	3.232 and −1.852

$^{31}P\{^1H\}$ NMR spectra of the tin complexes show splitting due to ^{31}P–Sn coupling in all cases together with ^{31}P–^{77}Se coupling in the case of **7**. Moreover, in $^{31}P\{^1H\}$ NMR spectra of **7**, phosphorus–carbon coupling was observed, which was proven by an additional ^{13}C NMR experiment.

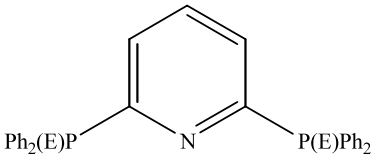

1. E = O (**2**)
2. E = S (**3**)
3. E = Se (**4**)

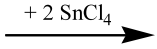

1. $[SnCl_3\{[Ph_2P(O)]_2C_5NH_3\}][SnCl_5(H_2O)]$ (**5**)
2. $[SnCl_3\{[Ph_2P(S)]_2C_5NH_3\}][SnCl_5]$ (**6**)
3. $[SnCl_3\{[Ph_2P(Se)]_2C_5NH_3\}][SnCl_5]$ (**7**)

(2)

Crystals suitable for X-ray structure determination were usually obtained by cooling the reaction mixtures and the crystals of **1** were obtained by the slow diffusion of methanol into a dichloromethane solution of **1**. Compound **2** crystallized as the peroxohydrate. Crystal data and refinement parameters are shown in Table 1. Unlike in the corresponding imidodiphosphinates, there are no hydrogens suitable for hydrogen bonding present in the ligand molecules. While many imidodiphosphinates and related compounds form hydrogen-bonded polymers or dimers in the solid state [9], there are no especially short intermolecular contacts in **1**, **3** and **4**. In the crystal packing of **2**, the intermolecular connection is allowed through the molecules of hydrogen peroxide, which leads to a chain arrangement (Fig. 1).

The ligand molecules adopt twofold internal symmetry in general, with the symmetry axis connecting

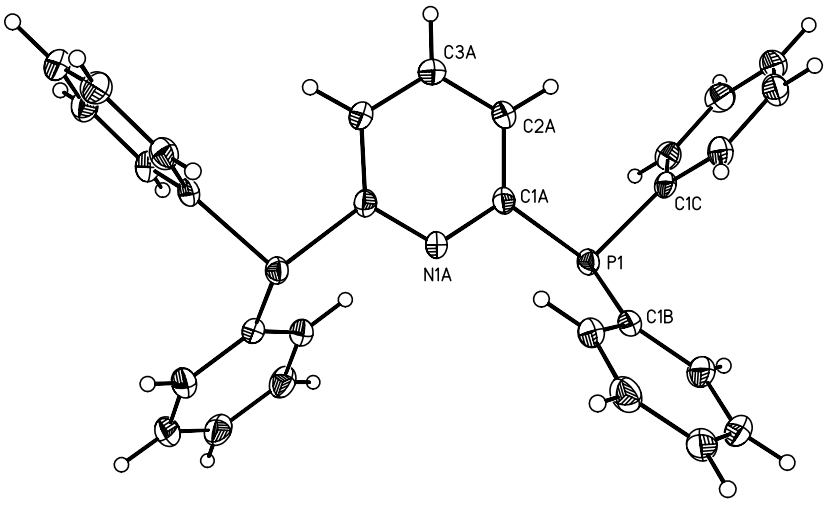

Fig. 1. An ORTEP representation of **1** showing the atom labelling scheme; atom contours are drawn at 50% probability level.

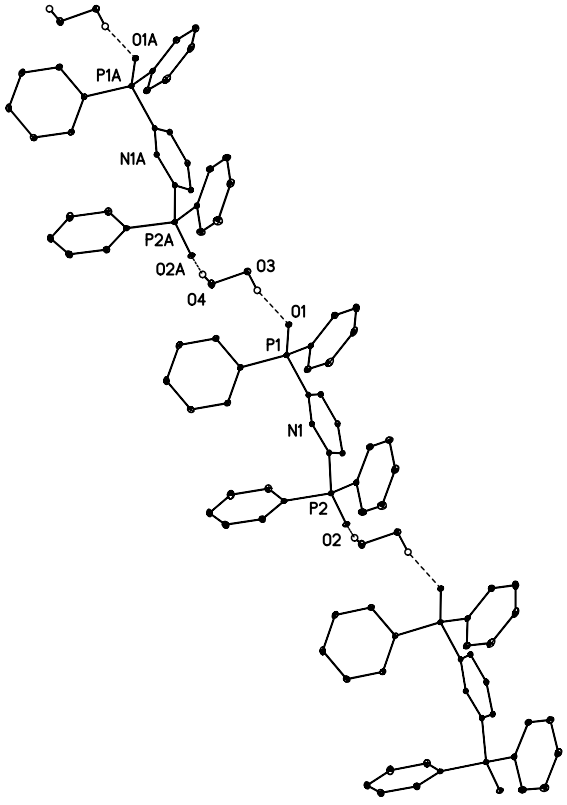

Fig. 2. The crystal packing of **2** showing the intermolecular contacts of $[Ph_2P(O)\text{-}C_5H_3N\text{-}P(O)Ph_2]$ with molecules of hydrogen peroxide.

nitrogen and the opposite carbon vertex in pyridine. The central pyridine part including both phosphorus atoms is nearly planar in all ligands, with the biggest mean deviation from calculated least-squares planes being 0.0476 Å in **1**. The terminal chalcogen atoms in oxidized derivatives are more or less deviated from these planes—the most deviating are seleniums in **3** (−0.749(2) and 0.736(2) Å) and the least are oxygens in **2** (−0.161(2) and 0.171(2) Å). While in **1** the Ph_2P groups have arbitrary orientation with respect to the pyridine center thus suggesting that they are easily rotated around the P–C bonds, the position of the sterically more demanding $Ph_2P(E)$ groups seems to be more organized. In all three cases, the P=E bonds tend to align with the pyridine plane (see above) and always point up towards the rest of the pyridine frame such that the phenyl substituents are located below nitrogen (Figs. 3 and 4). Both chalcogens are therefore far away from each other as well as from the lone electron pair of the nitrogen, and phenyl groups do not interfere with pyridine, all pendants thus taking spatially more favorable positions. It must be noted, however, that the chalcogens must take opposite orientation when acting in chelation as clearly seen from the present Sn(IV) complexes. This is also supported by involving the nitrogen electron pair in coordination, which is probably the most important barrier of the analogous arrangement of chalcogens in both complex and free ligands.

Selected bond lengths and angles are listed in Table 2. In P(V) ligands, the P–C bonds pointing to phenyl rings are shortened by oxidation of **1** and they become even shorter in Sn(IV) complexes. Either identical or opposite trends in P1–C1A and P2–C5A bonds connecting $Ph_2P(E)$ groups to pyridine are not observed. The phosphorus–chalcogen bonds are prolongated upon coordination in complexes **5**, **6** and **7**. The ligands derived from bppp have two $Ph_2P(E)$ groups connected through P–C and C–N bonds via a disubstituted pyridine. There is no through-conjugation involving the central electron-donating groups like in deprotonated $[E\text{–}P\text{–}N\text{–}P\text{–}E]^-$ chains (E = O, S, Se) of imidodiphosphinates [5,9]. Thus, as in the corresponding imidodiphosphinates, the phosphorus–chalcogen bond distances are lengthened upon complex formation, while

Table 2
Selected bond lengths (Å) and angles (°) for ligands **1**–**4** and Sn(IV) compounds **5**–**7**

	1 [a]	**2**	**3**	**4**	**5**	**6**	**7**
Bond lengths							
P1–E1		1.483(1)	1.941(6)	2.097(1)	1.525(3)	1.989(2)	2.136(3)
P2–E2		1.475(1)	1.943(6)	2.097(1)	1.514(3)	1.992(2)	2.144(3)
P1–C1A	1.832(1)	1.810(2)	1.826(2)	1.829(2)	1.816(5)	1.822(4)	1.832(11)
P2–C5A		1.804(2)	1.823(2)	1.829(2)	1.827(4)	1.819(4)	1.824(10)
C1A–N1A	1.348(1)	1.339(2)	1.332(2)	1.333(3)	1.344(6)	1.335(5)	1.337(13)
C5A–N1A		1.338(2)	1.334(2)	1.336(3)	1.343(6)	1.336(5)	1.345(13)
P1–C1B	1.821(1)	1.789(2)	1.805(2)	1.803(2)	1.775(5)	1.774(4)	1.790(11)
P1–C1C	1.822(1)	1.791(2)	1.806(2)	1.811(2)	1.763(5)	1.778(4)	1.786(11)
P2–C1D	1.821(1)	1.783(2)	1.806(2)	1.811(2)	1.776(5)	1.792(4)	1.789(11)
P2–C1E	1.822(1)	1.788(2)	1.810(2)	1.810(2)	1.769(5)	1.773(4)	1.775(10)
Sn1–E1					2.085(3)	2.503(1)	2.630(1)
Sn1–E2					2.091(3)	2.514(1)	2.599(1)
Sn1–N1A					2.235(4)	2.287(3)	2.305(8)
Sn1–Cl1					2.308(1)	2.339(1)	2.351(3)
Sn1–Cl2					2.369(1)	2.372(1)	2.392(3)
Sn1–Cl3					2.362(1)	2.387(1)	2.392(3)
Bond angles							
E1–P1–C1A		110.49(8)	112.62(5)	112.24(8)	104.6(2)	111.8(1)	111.4(3)
E2–P2–C5A		111.24(8)	113.05(6)	113.15(8)	105.4(2)	111.1(1)	111.3(3)
P1–C1A–N1A	114.6(1)	116.1(1)	114.3(1)	114.4(2)	125.1(3)	119.2(3)	120.1(8)
P2–C5A–N1A		115.3(1)	113.1(1)	113.1(2)	112.7(3)	119.9(3)	122.4(7)
N1A–Sn1–Cl1					177.29(9)	177.61(9)	179.3(2)
Cl2–Sn1–Cl3					169.85(4)	167.51(4)	167.6(1)
E1–Sn1–E2					157.8(1)	174.10(4)	176.75(4)
E1–Sn1–N1A					78.8(1)	87.72(8)	88.0(2)
E2–Sn1–N1A					79.1(1)	86.95(8)	88.8(2)

[a] Only half of a molecule forms an asymmetric unit.

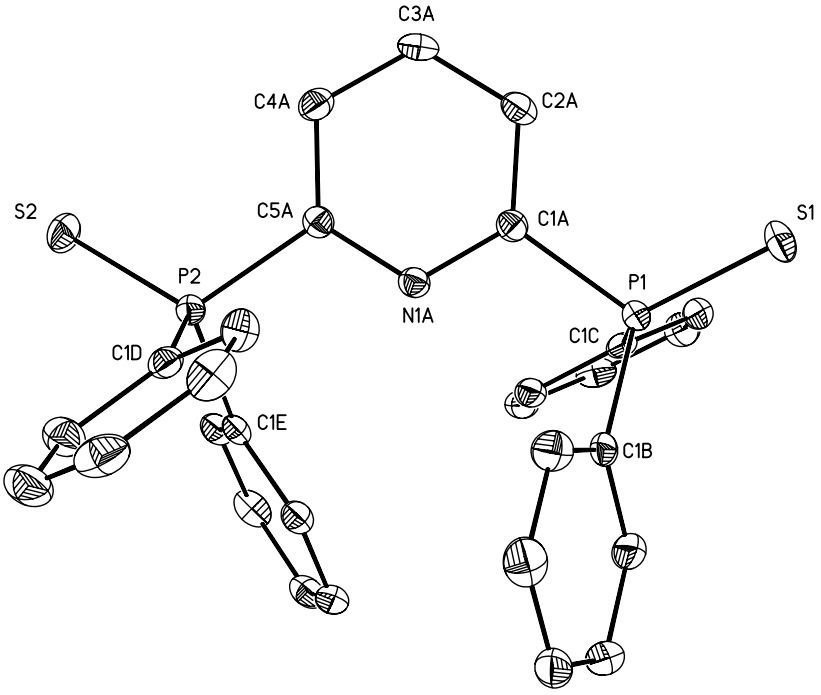

Fig. 3. An ORTEP representation of **3** showing the atom labelling scheme; atom contours are drawn at 50% probability level and hydrogen atoms are omitted for clarity.

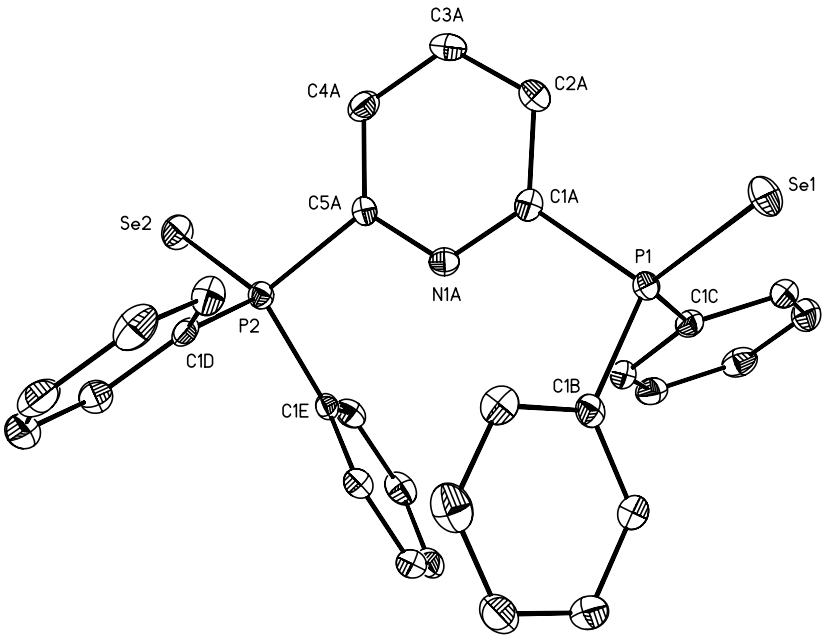

Fig. 4. An ORTEP representation of **4** showing the atom labelling scheme; atom contours are drawn at 50% probability level and hydrogen atoms are omitted for clarity.

the other changes throughout the chelate rings are unimportant on the other hand (in imidodiphosphinate ligands, the delocalization occurring in the chelate rings is also responsible for the shortening of P–N bonds).

Each of the oxidized ligands was allowed to react with $SnCl_4$ to give a set of heteroleptic complexes with a chelating molecule of $Ph_2P(E)$-C_5H_4N-$P(E)Ph_2$, and three chlorine atoms around Sn(IV) in the cationic part and five chlorines (and an aqua ligand in **5**) around another Sn(IV) center in the anionic part. The structures of the prepared complexs **5**, **6** and **7** are shown in Figs. 5–7. The cations show approximate octahedral core geometry, which is most distorted in the oxygen derivative. Apparently, this is due to two factors: (a) the presence of the Sn–N bond, which cannot be too compressed without inducing some repulsion between nuclei and (b) the small radii of oxygens, which do not allow the ligand to get closer to the tin without Sn–N bond compression and/or excessive lengthening of P–O bond distances. Thus, the conflict is solved mainly by a decrease in O–Sn–N bond angles of approximately 10° compared to **6** and **7**. To avoid the different *trans* influence, **5** can be most appropriately compared to the structurally similar compound $[(EtO)_2P(O)$-$(t$-$Bu)C_6H_3$-$P(O)(OEt)_2]SnCl_3$, where a carbon atom takes the donating role of nitrogen in **5**, and the O–Sn–O angle is distorted in a similar manner (161.1°) [10]. In another two compounds with SnO_2Cl_3C central cores, trichloro-bis(hexamethylphosphoric triamide)-phenyl-tin and ethyl-trichloro-bis(triphenylphosphine oxide)-tin, where tin

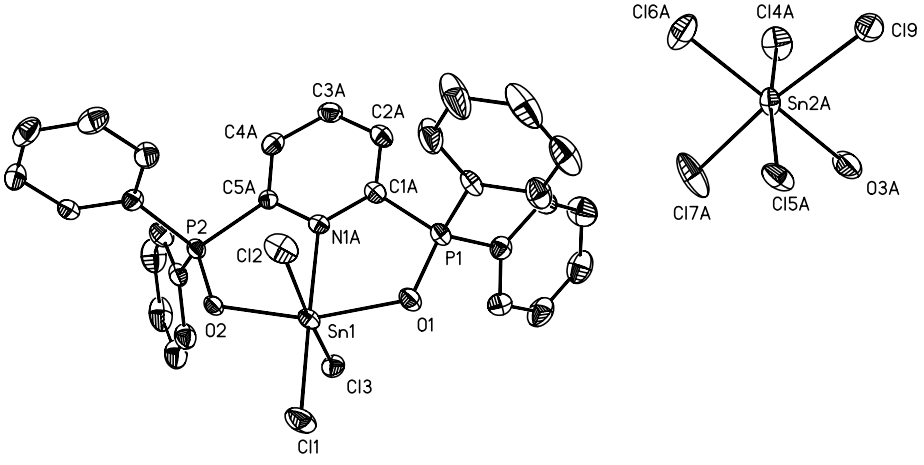

Fig. 5. An ORTEP representation of **5**; atom contours are drawn at 50% probability level; hydrogen atoms and dichloromethane solvate molecule are omitted for clarity.

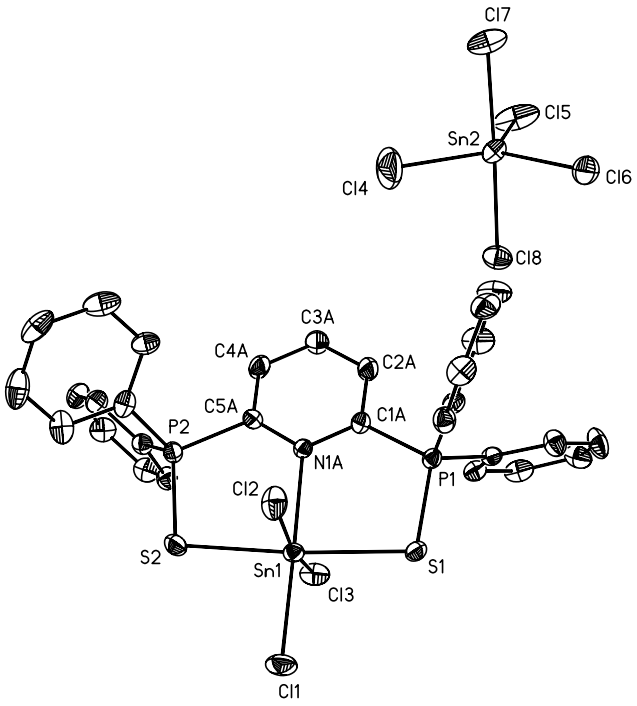

Fig. 6. An ORTEP representation of **6**; atom contours are drawn at 50% probability level; hydrogen atoms and dichloromethane solvate molecule are omitted for clarity.

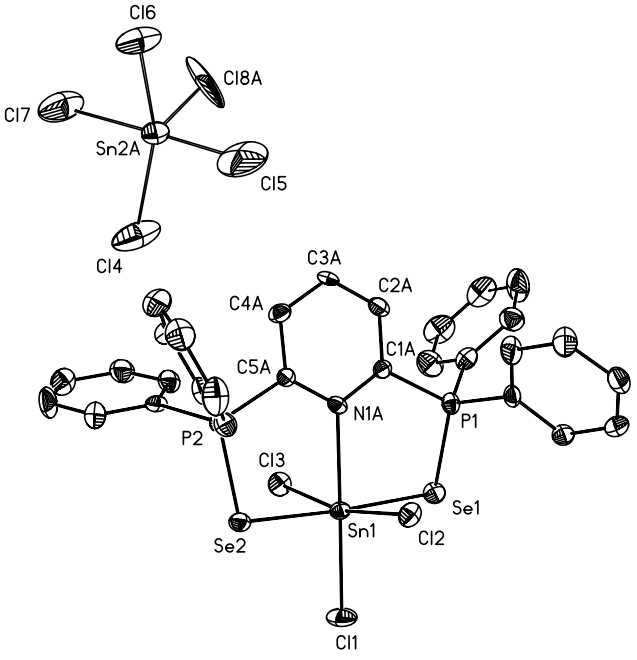

Fig. 7. An ORTEP representation of **7**; atom contours are drawn at 50% probability level; hydrogen atoms and dichloromethane solvate molecules are omitted for clarity.

is surrounded by six monodentate ligands (three Cl, one Ph or Et, two *trans*-positioned either $(Me_2N)_3PO$ or Ph_3PO), the Sn–O bonds are almost co-linear (O–Sn–O angles: 176.0° and 178.6°, respectively) [11,12]. Undoubtedly, the restricted sterical relations between donor atoms in chelating ligands are responsible for deviations from an octahedral geometry. It is interesting to note that the corresponding bond lengths are systematically shorter in **5** than in $[(EtO)_2P(O)\text{-}(t\text{-}Bu)C_6H_3\text{-}P(O)(OEt)_2]SnCl_3$ (about 0.13 Å for Sn–O and 0.1 Å for Sn–Cl bonds), which can be most probably attributed to the lack of electrons in the valence shell of the central Sn(IV) in **5** after Cl^- displacement. While $(EtO)_2P(O)\text{-}(t\text{-}Bu)C_6H_3\text{-}P(O)(OEt)_2^-$ compensates for this electron deficiency with its negative charge, the $bpppO_2$ ligand is neutral in the cationic chelate **5**, and the neighboring atoms get closer to the tin due to its enhanced Lewis acidity.

In spite of remarkable distortion of the coordination polyhedron in **5**, additional Sn–N bond shortening can be noticed. In the series of our three Sn(IV) complexes, the Sn–N bond in **5** is about 0.07 Å shorter in comparison to the appropriate bond in **7**. The spatial relations in the Sn(IV) cations are also reflected in the planarity of the chelate rings. In the selenium derivative, which has the longest P–E distances among the three complexes, its two P–Se bonds need not be aligned (the Se–P···P–Se "torsion angle" being 27.0(1)°) while still allowing almost regular octahedral geometry around tin. In both other complexes, the planes calculated through the chelate rings show only insignificant mean deviations of included atoms (0.0391 Å in **5** and 0.0715 Å in **6** against 0.1538 Å in **7**).

In all complexes, the chlorine situated *trans* to the nitrogen is slightly but significantly shifted towards tin than the neighboring two chlorines. The differences between Sn–Cl1 and the other two Sn–Cl bonds average are 0.058, 0.041 and 0.041 Å in **5**, **6** and **7**, respectively. This can be viewed as a result of a smaller *trans* influence of the chelating ligand related to its weaker donating properties than that of the opposite chlorine. Along with the Sn–N bond shortening and reducing the atomic radii of the chalcogen donors from **7** to **5**, the Sn–Cl bonds also become progressively shorter.

The Sn(IV) anionic counterparts are mutually different in their nature and geometry. While in **6** and **7** the $[SnCl_5]^-$ unit forms more or less a regular trigonal bipyramid, in **5** it adopts a water molecule in the coordination sphere to take octahedral geometry. The anions in **5** and **7** are affected by significant disorder causing irregularities in bond lengths and angles, thus making the precise structural study difficult. In the $SnCl_5(OH_2)^-$ anion, the O–Sn–Cl bond angles (involving chlorines non-opposite to oxygen) are compressed, varying from 84.2(3)° to 88.1(2)°. This distortion is similar to what is found in other crystallographically characterized $SnCl_5O$ cores in either $SnCl_5(OH_2)^-$ or $SnCl_5(thf)^-$ anions [4].

In conclusion, after a long time intensive study of simple diphosphinate ligands with simple central bridging groups like –NH– or $-(CH_2)_n-$, their more

complicated variations with larger bridges like aniline [13] and ferrocene [14] were presented recently. These ligands bring more flexibility in their skeletons (ferrocene) leading to a variety of coordination modes on the one hand and the more compact frames (pyridine) with more restricted coordination geometries on the other.

7. Supplementary material

Crystallographic data for the structural analysis have been deposited with the Cambridge Crystallographic Data Centre, CCDC Nos. 198667–198673. Copies of this information may be obtained free of charge from The Director, CCDC, 12 Union Road, Cambridge, CB2 1EZ, UK (fax: +44-1223-336033; e-mail: deposit@ccdc.cam.ac.uk or www: http://www.ccdc.cam.ac.uk).

Acknowledgements

This work was supported by the Grant Agency of the Czech Republic (grant No. 203/02/0436) and by the Ministry of Education of the Czech Republic (MSM 143100011).

References

[1] F.A. Cotton, E.V. Dikarev, G.T. Jordan, IV, C.A. Murillo, M.A. Petrukhina, Inorg. Chem. 37 (1998) 4611.
[2] G.R. Newkome, D.C. Hager, J. Org. Chem. 43 (1978) 947.
[3] H.Ch.E. McFarlane, W. McFarlane, A.S. Muir, Polyhedron 9 (1990) 1757.
[4] F.H. Allen, O. Kennard, 3D search and research using the Cambridge structural database, Chem. Des. Automation News 8 (1993) 1, 31.
[5] T.Q. Ly, J.D. Woollins, Coord. Chem. Rev. 176 (1998) 451.
[6] D.D. Perrin, W.L.F. Armarego, Purification of Laboratory Chemicals, Pergamon Press, Oxford, 1988.
[7] Oxford Diffraction Ltd., Xcalibur CCD System, CrysAlis Software System, Version 1.168, Oxford, UK, 2001.
[8] SHELXTL, Version 5.10, Bruker AXS, Inc., Madison, WI, 1997.
[9] P. Bhattacharyya, J.D. Woollins, Polyhedron 14 (1995) 3367.
[10] M. Mehring, C. Low, M. Schurmann, K. Jurkschat, Eur. J. Inorg. Chem. (1999) 887.
[11] A.V. Yatsenko, S.V. Medvedev, L.A. Aslanov, Zh. Strukt. Khim. 33 (1992) 126.
[12] A.I. Tursina, L.A. Aslanov, S.V. Medvedev, A.V. Yatsenko, Koord. Khim. 11 (1985) 417.
[13] Q. Zhang, S.M. Aucott, A.M.Z. Slawin, J.D. Woollins, Eur. J. Inorg. Chem. (2002) 1635.
[14] M. Necas, M. Beran, J.D. Woollins, J. Novosad, Polyhedron 20 (2001) 741.